OPEN ACCESS Freely available online

Journal of Physical Chemistry & Biophysics

Research Article

A Novel Solution for Rapid Auto-Focusing in Dynamic Imaging Scenarios

Xiao Zhiyuan, Hu Shenming*, Sun Yuchen, Li Lei, Zhao Hongyu

Department of Medicine and Biological Information Engineering, Northeastern University, Shenyang, China

ABSTRACT

In dynamic imaging scenarios and precision applications requiring rapid refocusing, traditional imaging systems often struggle to maintain sharp and accurate images. To address these challenges, we propose a solution that integrates the Single-Aberration Focusing Lens Inspired by Human Eye Crystals (SAFLE-HEC) with a custom algorithm to enhance both dynamic imaging and precision applications. The SAFLE-HEC lens achieves rapid focus adjustments, with average autofocus times of 10.92 ms in static and 16.81 ms in dynamic scenarios, while maintaining image clarity. Additionally, the lens performs robustly under challenging lighting conditions, including underexposure and overexposure, and demonstrates high accuracy in object tracking. The real-time tracking algorithm allows QR code detection to be completed in under 2 ms. In high-speed turntable tests at 300 rpm, autofocus time increased slightly but remained under 20 ms, and QR code detection stayed under 4 ms. This hardware-software integrated solution provides a cost-effective and efficient option for machine vision, particularly in automated quality inspection and real-time tracking in industrial environments.

Keywords: Imaging scenarios; Machine vision; Overexposure; Algorithm

INTRODUCTION

In the study of dynamic imaging scenarios, ensuring consistent image clarity and accuracy presents a significant challenge due to the continuous changes in objects or scenes. As such, autofocus and dynamic tracking technologies play a crucial role in addressing these challenges. In the field of Autofocus, researchers from around the world have conducted research and achieved notable results. In their study, Jiang employed a ResNet50 convolutional neural network to process the input defocus image and subsequently output the distance between the current object surface and the focal plane. Yang SJ implemented a classification network model by measuring the defocus of biological cell microscopy images. Nevertheless, the detection of the focal plane is not sufficiently precise, thereby rendering it challenging to apply it to high-precision equipment. Wu et al., proposed a deep learning-based refocusing algorithm that is capable of refocusing a 2D fluorescence microscopy image to a specified imaging plane, effectively reconstructing a 3D image from a 2D microscopy image. Pinkard et al., proposed a self-collimation method based on correlated illumination light. This method entails modifying the light source of the imaging system, employing coherent illumination and ultimately utilising a data-driven deep convolutional neural network for model training and learning. Dastidar et al., put forward a methodology whereby a lightweight network serves as the foundation for an Autofocus convolutional neural network. This approach enables the prediction of the defocus distance of the current input image, with the input comprising a difference image of two defocus images with a fixed spacing of 2 μm. Herrmann et al. proposed a modern deep classification model and ordered regression loss to obtain an effective deep neural network-based autofocus technique. Luo et al. applied a deep learning-based offline autofocus method to achieve single-shot microscope image autofocus for specimens captured in any defocus plane. Liao et al., devised an enhanced version of MobileNetV3 for the purpose of predicting the defocus distance of a single microscope image that had been acquired on an arbitrary image

Correspondence to: Hu Shenming, Department of Medicine and Biological Information Engineering, Northeastern University, Shenyang, China, Tel: 9876543210; E-mail: hushenming3@sina.com

Received: 18-Dec-2024, Manuscript No. JPCB-24-35963; **Editor assigned:** 23-Dec-2024, PreQC No. JPCB-24-35963 (PQ); **Reviewed:** 06-Jan-2025, QC No. JPCB-24-35963; **Revised:** 12-Jan-2026, Manuscript No. JPCB-24-35963 (R); **Published:** 19-Jan-2026, DOI: 10.35841/2161-0398.26.16.442

Citation: Zhiyuan X, Shenming H, Yuchen S, Lei L, Hongyu Z (2026) A Novel Solution for Rapid Auto-Focusing in Dynamic Imaging Scenarios. J Phys Chem Biophys. 16:442.

Copyright: © 2026 Zhiyuan X, et al. This is an open-access article distributed under the terms of the Creative Commons Attribution License, which permits unrestricted use, distribution, and reproduction in any medium, provided the original author and source are credited.

plane. This defocus prediction process was completed in a mere 9 ms. Teng et al., improved the sharpness evaluation function by introducing Gaussian filtering and a threshold-controlled Laplace operator, which were combined with coarse and fine-tuning search strategies to achieve accurate and reliable focusing [1,2].

Despite the considerable advancements in autofocus technology observed in traditional optical lenses, these lenses remain bulky in size, exhibit a prolonged focusing response time and are susceptible to friction. The use of liquid lens autofocus technology serves to overcome the shortcomings and limitations of traditional optical focusing systems. This is achieved by taking advantage of the deformable properties of liquid materials, which allows for fast and precise Autofocusing to be achieved by adjusting the internal parameters of the optical elements through external control, without any mechanical parts moving. The application of liquid lenses in diverse fields has been a topic of considerable interest, particularly with regard to the enhancement of their focusing rate. For a period extending beyond a decade, researchers have achieved significant advances in the development of high-speed focusing techniques for liquid lenses. Zhang et al. developed a liquid lens-based dual-beam laser autofocus system with 'time-sharing focusing and fast switching' for rapid focusing, reducing the autofocusing time to approximately 10 ms. Fricke et al., put forward a non-contact dermatoscope based on the auto-focus function of a liquid lens for application in routine skin cancer screening. Lan et al., suggested a liquid crystal lens hill-climbing autofocus algorithm as a potential solution to the limitations of traditional focusing systems, which are characterised by mechanical movement and high power consumption. Berthelon argued that the deployment of liquid lens technology could facilitate the overcoming of the optical limitations of conventional systems, thereby enabling the achievement of rapid autofocus and enhanced imaging clarity in iris recognition systems. Liu et al., advanced a rapid autofocus methodology for bionic vision, based on liquid lenses, to address the shortcomings of conventional imaging systems with respect to focusing precision and velocity. Karkhanis et al., exploited the liquid lens autofocus functionality to achieve the greatest possible restoration of patients diagnosed with presbyopia to the level of accommodation that would have been attained had the patients' eyes remained healthy. Liu et al., posited an autofocus strategy based on liquid lens focus shift as a means of addressing the issue of an underwater hyperspectral imager's inability to focus due to distance fluctuations. Budd et al., incorporated a focusable liquid lens into a video hyperspectral imager. A video autofocus method based on deep reinforcement learning was proposed for an imaging borescope. Zhang et al., achieved high-speed and high-precision autofocus through the application of liquid lens technology, which in turn promoted the development of high-magnification target tracking technology [3-5].

In conclusion, in dynamic imaging scenarios where precise and rapid refocusing is critical, traditional systems often fall short in maintaining image clarity. To overcome this challenge, we propose a novel solution that combines the Single-Aberration Focusing Lens Inspired by Human Eye Crystals (SAFLE-HEC) with a custom-developed algorithm for real-time adaptive focus adjustment. The solution integrates the lens hardware's ability to quickly accommodate varying distances with the algorithm's capacity to dynamically optimize focus in response to environmental changes. This dual-component solution provides an innovative approach to high-speed, high-precision imaging in dynamic applications.

MATERIALS AND METHODS

The principles of autofocus

Autofocus is the process by which an optical system is continuously adjusted to uphold the relationship between object and image positions as prescribed by imaging theory, thus yielding a sharp image, as shown in Figure 1. Let p denote a point on the object plane, μ the distance from p to the center of the lens, ν the distance from the focused image point p′ to the center of the lens, s the distance from the lens center to the image detector, D the lens aperture diameter, and R the radius of the blurred image point p′ on the image detector. According to the principles of geometrical optics, imaging with a thin lens adheres to the Gaussian formula, as shown below [6].

$$\frac{1}{\mu}+\frac{1}{v}=\frac{1}{f} \qquad \text{[Eq.(1)]}$$

When the optical system is precisely focused, the object-image relationship satisfies the above equation, resulting in an ideal image with the image point denoted as p′. However, when the imaging system is disrupted, meaning that the values of μ or ν change, a blurred image point forms on the detector. The shape of the blurred image point resembles that of the lens aperture, and its size is proportional to the diameter of the lens aperture. As the distance between the detector and the focal plane increases, indicated by a larger value of s−ν, the size of the blurred image point on the detector also increases, reflecting greater defocus in the optical system. In a defocused state, it can be inferred from the similar triangles in Figure 1 that the following relationship holds.

$$\frac{DR}{2}=\frac{s-v}{v}=s\left(\frac{1}{v}-\frac{1}{s}\right) \qquad \text{[Eq.(2)]}$$

From the above two equations, it can be derived that.

$$R=\frac{Ds}{2}\left(\frac{1}{f}-\frac{1}{\mu}-\frac{1}{s}\right)=\frac{Ds}{2}\left(\frac{1}{v}-\frac{1}{s}\right) \qquad \text{[Eq.(3)]}$$

According to Equation (2.3), when ν=s, R=0, indicating that the image plane is precisely at the focal plane. When ν<s, R>0, placing the image plane behind the focal plane, while ν>s results in R<0, positioning the image plane in front of the focal plane. Therefore, a clear image can be achieved by adjusting the values of μ, s, and f to align the image plane with the focal plane [7].

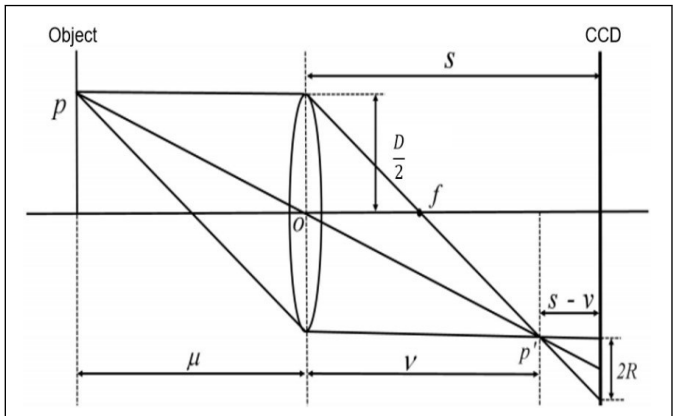

Figure 1: Imaging principle schematic diagram.

Adjustable working distance and working mechanism of SAFLE-HEC

As illustrated in Figure 2, conventional fixed-focus lenses present limitations due to their reliance on time-consuming mechanical adjustments for each specific object height, which restricts their adaptability and working distance in dynamic environments. This approach requires frequent manual intervention, making it less efficient and more cumbersome for applications demanding rapid changes in focal length. In contrast, SAFLE-HEC lens offers a technologically advanced solution by eliminating the need for mechanical refocusing. Its rapid and seamless focusing capability enhances operational efficiency, providing a broader working range that adapts more flexibly to varying object distances and heights, thus meeting the demands of dynamic imaging scenarios and precision-driven applications [8,9].

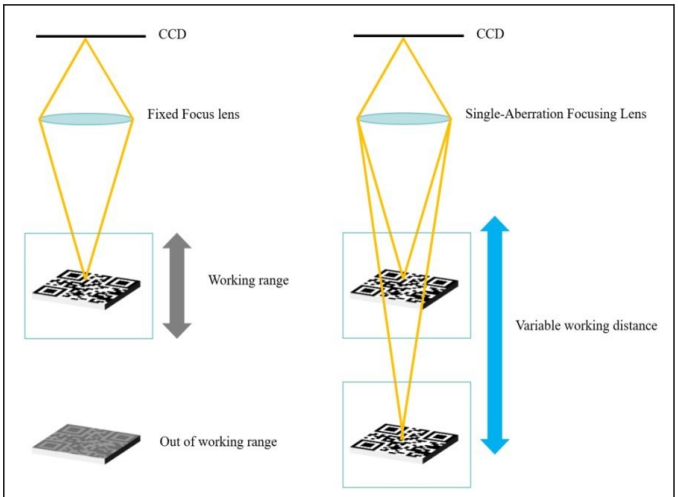

Figure 2: Comparison of working distances of lenses.

As illustrated in Figure 3, SAFLE-HEC lens is a compact optical component that contains an optical-grade liquid. The process begins with a command issued by a host computer to alter the focal power of the lens. Subsequently, a motor rotates to move the actuator, which either pushes or retracts the lens assembly. This movement causes the liquid to change the shape of the lens. This transformation occurs within milliseconds and results in a variation of the lens's optical power, thereby changing its focal length and working distance. When the axis head is pushed inward, the lens exhibits the characteristics of a convex lens; conversely, when it is retracted, the lens demonstrates the properties of a concave lens.

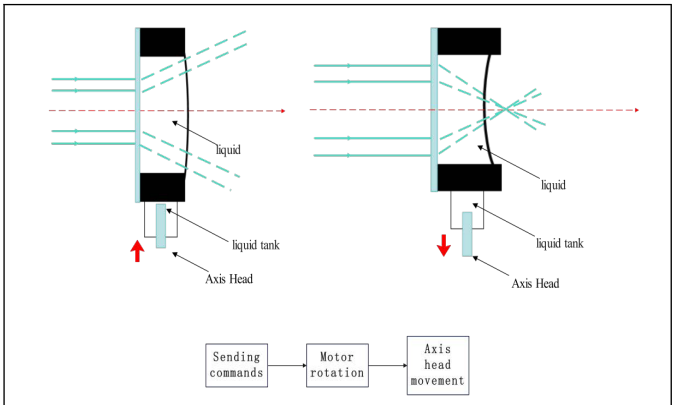

Figure 3: Working mechanism of SAFLE-HEC.

As shown in Figure 4. The proposed solution is an integrated hardware-software system designed to address the challenges of rapid and precise focusing in dynamic imaging scenarios. The system consists of two core components: The SAFLE-HEC lens and real-time autofocus, along with a QR code detection and recognition algorithm. Within the system, the SAFLE-HEC lens and our developed algorithms work in close synergy to ensure high-speed and high-precision imaging performance. The hardware provides the foundation for rapid focus adjustments, while the algorithm dynamically computes and adjusts the focus in real-time to accommodate variations in lighting, object movement, and other environmental factors. The collaboration between these two components enables precise tracking and rapid focusing on objects within dynamic environments.

Figure 4: Hardware-software interaction in our solution.

Tenengrad gradient function

Tenengrad image sharpness evaluation function is an index used for image quality assessment, primarily employed for detecting image sharpness. It evaluates image sharpness by analyzing the intensity of gradients within the image. A higher gradient amplitude indicates a sharper image.

Based on the concept of edge detection, the Tenengrad function utilizes the Sobel operator to compute the image gradients in both the horizontal and vertical directions. To amplify the gradient information at the edges of the image, the gradient values are squared.

$$AOV_{Ten} = \sum_x \sum_y [G(x,y)]^2 \quad \text{[Eq.(4)]}$$

Where AOV_{Ten} denotes the evaluation value, while G(x, y) represents the gradient at the pixel coordinates (x, y).

$$G(x,y) = \sqrt{G_x^2(x,y) + G_y^2(x,y)} \quad \text{[Eq.(5)]}$$

Where G_x(x, y) denotes the horizontal gradient of the pixel, G_y(x, y) denotes the vertical gradient of the pixel.

$$G_x(x,y) = f(x,y) \otimes g_x \quad \text{[Eq.(6)]}$$
$$G_y(x,y) = f(x,y) \otimes g_y \quad \text{[Eq.(7)]}$$

Where ⊗ denotes the convolution operator symbol, g_x denotes the horizontal Sobel operator, g_y denotes the vertical Sobel operator.

$$g_x = \begin{bmatrix} 1 & 0 & -1 \\ 2 & 0 & -2 \\ 1 & 0 & -1 \end{bmatrix} \quad g_y = \begin{bmatrix} 1 & 2 & 1 \\ 0 & 0 & 0 \\ -1 & -2 & -1 \end{bmatrix} \quad \text{[Eq.(8)]}$$

Building upon the Tenengrad function, an alternative enhancement method involves calculating the variance of gradient magnitudes. Based on this concept, a novel evaluation function methodology is derived.

$$AOV_{Tenvar} = \sum_x \sum_y [G(x,y) - \bar{G}]^2 \quad \text{[Eq.(9)]}$$

Where, AOV_{Tenvar} denotes the evaluation value, $\bar{G}$ denotes the mean value.

$$\bar{G} = \frac{1}{xy} \sum_x \sum_y G(x,y) \quad \text{[Eq.(10)]}$$

RESULTS AND DISCUSSION

The experiments were conducted on a computer powered by an Intel Core i9-13900K processor, with 32 GB of DDR4 RAM and a 1 TB SSD. The system operated on a 64-bit version of Windows 11 Pro. The computational environment was set up with Halcon 23.11. Following the description of the software environment, the hardware environment for the experiments is as follows: GFL-Z400-RS485 laser displacement sensor (Dongguan Dadisick Co., Ltd, China), FA lens (25 mm, F2.4, 1/1.8, Hangzhou Hikrobot Co., Ltd, China), industrial camera (Hangzhou Hikrobot Co., Ltd, China), and RH-MVT4-900-1 machine vision experimental stand (Shanghai Rechi Automation Technology Co., Ltd., China).

To evaluate the performance of the SAFLE-HEC lens in dynamic imaging scenarios, we integrated it with a dynamic imaging scenarios for automated quality inspection tasks. The system was tested at various working distances, ranging from 200 mm to 600 mm, to assess the lens's ability to rapidly adjust focus as the distance and height of the objects changed. As shown in Table 1, the lens was able to quickly and stably adjust its focus across the working distance range from 200 mm to 600 mm (The measurement error in each segment is confined to a maximum of 2 mm), with no noticeable decrease in image quality, as the average value calculated using the Tenengrad Gradient Function ($\bar{G}$) was 122.225 and the SAFLE-HEC lens was able to adjust focus in under an average of 10.924 milliseconds (T_1) while maintaining high image clarity throughout the test, even as the working distance fluctuated. In particular, the lens performed exceptionally well in rapidly adapting to changes in working distance, consistently producing sharp, focused images across the entire working distance range. In comparison, contrast detection autofocus showed noticeable lag and occasional image blurring when the object distance changed quickly.

Table 1: Autofocus performance across different working distances using the SAFLE-HEC lens and CDAF.

Methods	Distance (ms)	$\bar{G}$	T_1(s)
CDAF	200	115.452	5.45
	300	113.286	6.33
	400	116.432	6.81
	500	118.054	5.74
	600	111.987	6.19
Our	200	121.467	0.01012

300	122.983	0.01146
400	122.755	0.01093
500	121.892	0.01087
600	122.178	0.01124

To evaluate the performance of the SAFLE-HEC lens in dynamic imaging scenarios, we conducted a simulation experiment of a dynamic imaging scenarios, as shown in Figure 4. The imaging system consists of an industrial camera, a FA camera, and the SAFLE-HEC lens. The working principle involves first acquiring the distance information. This distance data is then converted into the corresponding motor step size using a pre-established fitting function that relates the distance to the motor step size. The motor movement is controlled *via* a driver board, which adjusts the lens's focal plane position and the lower right corner of Figure 5 illustrates the performance of real-time Autofocus, along with the real-time QR code detection and recognition process.

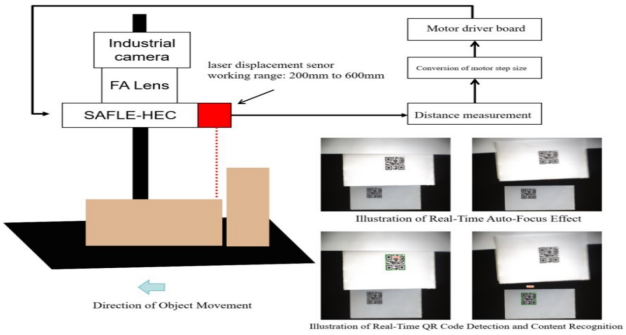

Figure 5: Schematic diagram of real-time autofocus and QR code recognition principles.

As shown in Table 2, in the simulated dynamic imaging scenarios, when the distance and position of objects remained stationary, the SAFLE-HEC lens responded quickly (T=0.41 s) and accurately adjusted its focus to maintain clear images ($\bar{G}$=124.507). In comparison with Manual Focus (MF) and CDAF, the SAFLE-HEC lens demonstrated faster response times and higher image stability. MF and CDAF often exhibited noticeable delays, whereas the SAFLE-HEC lens was able to make quick and precise focus adjustments under such conditions.

Table 2: Contrastive evaluation of three distinct focusing methods in static scenarios.

Focusing methods	$\bar{G}$	T(s)	Number of loops (times)
MF	101.377	7.11	None
CDAF	111.763	5.83	10~13
Our method	124.507	0.41	1

After validating the zoom response speed and autofocus time under static conditions with respect to image clarity for SAFLE-HEC, we proceeded to evaluate its performance in dynamic imaging scenarios. We set the exposure time of the FA lens to 30000.0, and configure the frame rate to 30.0 frames per second. As shown in Figure 6, these six images were captured during the process of evaluating its performance in dynamic imaging scenarios, ranging from 600 mm to 200 mm. The detection and recognition of the QR code took less than 2.1 ms. Additionally, the Autofocus operation was executed efficiently, with a time duration of no more than 17.7 ms.

Figure 6: Demonstration of autofocus and QR code detection and recognition at different distances.

Subsequently, we calculate the average values of $\bar{G}$, Autofocus time (T_d), and QR code detection and recognition time (T_{QR}) for each segment, with each segment corresponding to a 100 mm interval, spanning from 200 mm to 600 mm. The results are presented in Table 3. The maximum Autofocus time is observed in the 400-500 mm segment, reaching 17.6 ms, while the highest QR code detection and recognition time occurs in the same 400-500 mm segment, at 1.97 ms. Across the full frequency range from 200 mm to 600 mm, the average Autofocus time is 16.81 ms, and the average time for QR code detection and recognition is 1.83 ms. These findings highlight the system's strong real-time performance and robust dynamic tracking capability. As shown in Figure 5, the tracking accuracy remains acceptable, suggesting that the system effectively balances efficiency and accuracy in dynamic scenarios.

Table 3: Performance of SAFLE-HEC in dynamic imaging scenarios and dynamic scene tracking.

D (mm)	$\bar{G}$	T_d (ms)	T_{QR} (ms)
200-300	121.347	17.02	1.82
300-400	122.411	15.73	1.61
400-500	122.166	17.6	1.97
500-600	121.873	16.87	1.91
Full range (200-600)	121.949	16.81	1.83

Finally, we validated the robustness of the proposed solution. We tested the solution under both underexposure and overexposure conditions and found that the results were very promising, as shown in Figure 7. The solution performed well even in challenging lighting situations, maintaining reliable Autofocus and accurate QR code detection and recognition. These findings suggest that the solution is robust and capable of handling a wide range of exposure levels effectively.

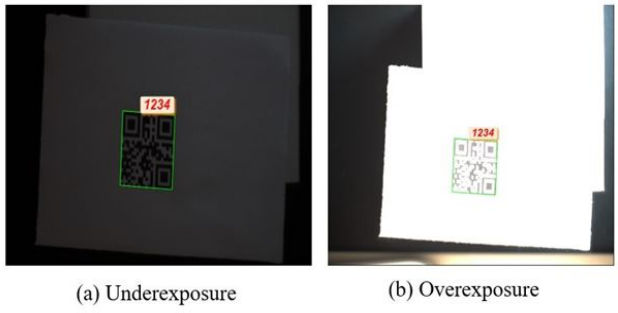

Figure 7: Autofocus and QR code dynamic tracking performance under different exposure levels.

Additionally, we conducted further experimental validation to assess the performance of the proposed solution. Tests were carried out on a turntable operating at 300 rpm, as shown in Figure 8, where we present the results for objects at two different heights on the high-speed rotating platform. Compared to a dynamic scene with simple Z-axis vertical movement control, both the average autofocus time and the QR code recognition time showed an increase. Specifically, the average autofocus time remained within 20 ms, while the QR code recognition and detection time was under 4 ms. The dashed box in the figure highlights the results captured by the algorithm. The QR code recognition results are indicated as '2431' and '1234' in the top-left corner of the image.

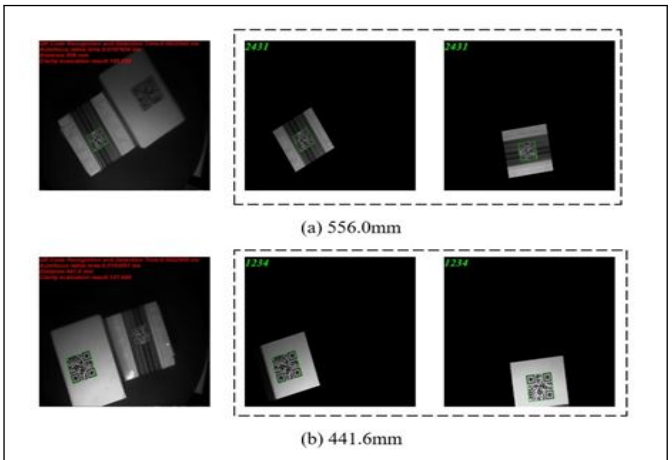

Figure 8: Autofocus and QR code recognition performance in a turntable scenario.

CONCLUSION

The experimental results demonstrate that the SAFLE-HEC lens, when integrated with our custom-developed algorithm, significantly outperforms conventional autofocus methods, such as CDAF and MF, in both static and dynamic imaging applications. In static tests, the SAFLE-HEC lens quickly and accurately adjusted focus across a wide working distance range of 200 mm to 600 mm, with an average autofocus time of just 10.92 milliseconds. In dynamic imaging scenarios, the lens exhibited exceptional performance, maintaining clear and sharp images while rapidly adjusting focus, even as object distance varied. The average autofocus time in dynamic tests was 16.81 milliseconds, with QR code detection and recognition times consistently under 2 milliseconds. Furthermore, the hardware-software integrated solution demonstrated robustness under challenging lighting conditions, including underexposure and overexposure, while maintaining reliable autofocus and precise QR code detection. Additionally, when tested in a high-speed turntable scenario at 300 rpm/min, the proposed solution showed a slight increase in both average autofocus time and QR code recognition time compared to the Z-axis vertical movement tests, but the values remained within acceptable limits. Specifically, the average autofocus time stayed under 20 ms, while the QR code recognition and detection time was under 4 ms. This increase in processing time did not compromise the system's accuracy or real-time capabilities.

These findings suggest that machine vision applications, especially those in high-volume assembly lines, require fast, accurate, and precise focusing to ensure high production throughput. By combining the SAFLE-HEC lens with our real-time tracking and autofocus algorithm, we provide a compact, cost-effective solution that delivers rapid focus adjustments across multiple distances, offering significant advantages for dynamic imaging tasks. This hardware-software integration represents a promising approach for real-time tracking, quality inspection, and other precision-critical applications in industrial environments.

STATEMENTS AND DECLARATIONS

The authors declare that they have no conflict of interest.

DATA AVAILABILITY

The original contributions presented in the study are included in the article, further inquiries can be directed to the corresponding author.

REFERENCES

1. Zhang Y, Liu L, Gong W, Yu H, Wang W, Zhao C, et al. Autofocus system and evaluation methodologies: A literature review. Sensors Material. 2018;30.
2. Jiang S, Liao J, Bian Z, Guo K, Zhang Y, Zheng G. Transform and multi-domain deep learning for single-frame rapid autofocusing in whole slide imaging. Biomed Opt Express. 2018;9(4):1601–1612.
3. Yang SJ, Berndl M, Michael Ando D, Barch M, Narayanaswamy A, Christiansen E, et al. Assessing microscope image focus quality with deep learning. BMC Bioinformatics. 2018;19(1):1–9.
4. Wu Y, Rivenson Y, Wang H, Luo Y, Ben-David E, Bentolila LA, et al. Three-dimensional virtual refocusing of fluorescence microscopy images using deep learning. Nat Methods. 2019;16(12):1323–1331.
5. Pinkard H, Phillips Z, Babakhani A, Fletcher DA, Waller L. Deep learning for single-shot autofocus microscopy. Optica. 2019;6(6):794–797.
6. Dastidar TR, Ethirajan R. Whole slide imaging system using deep learning-based automated focusing. Biomed Opt Express. 2019;11(1):480–491.
7. Luo Y, Huang L, Rivenson Y, Ozcan A. Single-shot autofocusing of microscopy images using deep learning. ACS Photonics. 2020;8(2):625–638.
8. Liao J, Chen X, Ding G, Dong P, Ye H, Wang H, et al. Deep learning-based single-shot autofocus method for digital microscopy. Biomed Opt Express. 2021;13(1):314–327.
9. Teng T, Guan C, Wang X, Fan H, Ju D, Chi Z. Autofocus optical imaging system based on image processing. Proc Int Conf Inf Opt Photonics. 2023:821–829.